5-2019

Autofluorescence to Study the Effects of Acid Concentration on Cellular Metabolism in Vitro

Robin L. Raley

Autofluorescence to Study the Effects of Acid Concentration on Cellular Metabolism in Vitro

An Honors Thesis submitted in partial fulfillment of the requirements of Honors Studies in Biochemistry

By

Robin L. Raley

Spring 2019

Department of Chemistry and Biochemistry

J. William Fulbright College of Arts and Sciences

The University of Arkansas

Fayetteville, AR

April 9, 2019

ACKNOWLEDGEMENTS

I would like to thank my advisor, Dr. Kyle Quinn, for his guidance, advice, and supportive reception of my joining his lab. I would also like to thank Hallie Ramser Toomer, who provided the Matlab codes for redox and FLIM analysis and conducted preliminary work on pig skin. Hallie acted as an indispensable research partner for follow up experiments (not included in detail in this thesis) and it was a privilege to learn from her. Additionally, I would like to thank my other graduate student mentor, Olivia Kolenc, for her expertise in cell culture and limitless patience.

TABLE OF CONTENTS

ABSTRACT

Ultraviolet (UV) radiation-induced sunburns and their accompanying afflictions are a growing public health concern in the United States. There is a need for techniques that can accurately and non-invasively characterize the physiology of sunburned skin tissue directly after UV-damage and applying a topical skin treatment to relieve pain and promote healing. Two-photon excited fluorescence (TPEF) microscopy and fluorescence lifetime imaging (FLIM) can be used to investigate metabolic processes in live cells through endogenous fluorescence of the cofactors, NADH and FAD. These methods employ the optical redox ratio of FAD/(NADH+FAD), mean NADH lifetime, and the separation of the free and bound NADH lifetime components to quantify glycolytic activity relative to oxidative phosphorylation. In this study, I probe the metabolism dynamics of mouse fibroblasts when treated with media containing increasing concentrations of an acid* as a first step to evaluate the effects of topical application of this acid to skin as a treatment for sunburns. I am able to show that significant increases in the redox ratio due to increasing Acid X treatment, in vitro, suggest that Acid X may shift metabolism in cells in a concentration-dependent manner. The application of methods here demonstrates that autofluorescence optical imaging can serve as a quantitative measure of cellular metabolism changes under the application of Acid X.

*Note: This acid will be referred to as “Acid X” throughout this thesis.

KEY WORDS: two-photon excitation, NADH, FAD, fluorescence, redox ratio, FLIM, sunburn

NOTE: This thesis work was conducted as part of a collaboration between the Quinn Lab and Dr. Jim Beckman of Therapon Inc.; aspects of this work may be included in a patent submission belonging to Dr. Jim Beckman. For this reason, proprietary details have been omitted throughout this thesis and have been replaced with unidentifiable names.

1. Introduction

Overexposure to ultraviolet (UV) radiation from natural sunlight or artificial sources can sunburn skin tissue and cause unpleasant symptoms such as soreness to the touch, itching, fluid-filled blisters, and inflammation. UV-induced skin damage alone is responsible for about 13 million cases of human keratinocyte skin cancers each year.[1] Additionally, the medical cost to treat skin cancer in the United States totaled to $1,452 million spent, at $1,209 per case, in 2014.[1] Increasingly, topical therapeutics are being researched and manufactured to provide relief and promote skin healing for minor sunburns.[2–5] Resolving the dynamics of how these treatments act on the wound site is critical to understanding the advantages and limitations that topical chemicals can contribute to this growing health problem.

Two-photon excitation fluorescence (TPEF) microscopy, is a fluorescence imaging technique that uses incident near-infrared (NIR) light to excite a sample. In contrast to traditional one-photon excitation (e.g. confocal microscopy) that involves excitation by one photon in the UV or visible light range, TPEF differs in that two NIR photons of double wavelength (lower energy) are absorbed simultaneously, which results in emission of a single photon by the fluorophore (a fluorescent molecule). Absorption of non-ionizing NIR light is preferred over harmful UV light when working with biological specimens. A comparison of the excitation-emission processes is shown schematically in **Figure 1**. Simultaneous photon absorption requires that the energy between a molecule's ground and excited states is less than the added energies of the two incident photons. When studying biological specimens such as cells, in vitro, total power deposition by the laser must be minimized. Therefore, lasers with ultrafast pulse repetition rates (80 MHz)

and small pulse width (<100 fs) for high peak power, such as the titanium-sapphire (Ti:Sapphire) laser used in this study, are ideal for biological imaging.[6] Additional advantages of TPEF that make it well suited for imaging biological samples include the following: (i) minimization of photodamage and scattering when compared to confocal microscopy, (ii) increased depth resolution as excitation is restricted to the focal plane of the microscope, (iii) minimization of out-of-focus fluorescence, and (iv) increased imaging depths enabled by NIR light penetration.[7,8] Photodamage is curtailed by the limited excitation volume at the focal plane, and scattering within the sample decreases with increasing wavelength as the gap between the excitation and emission spectra widens.[9] In this study, I utilize TPEF microscopy as a powerful tool to evaluate possible metabolic changes, in vitro, that involve administration of a chemical, referred to here as "Acid X", used in a nationally distributed skin care ointment to treat sunburns.

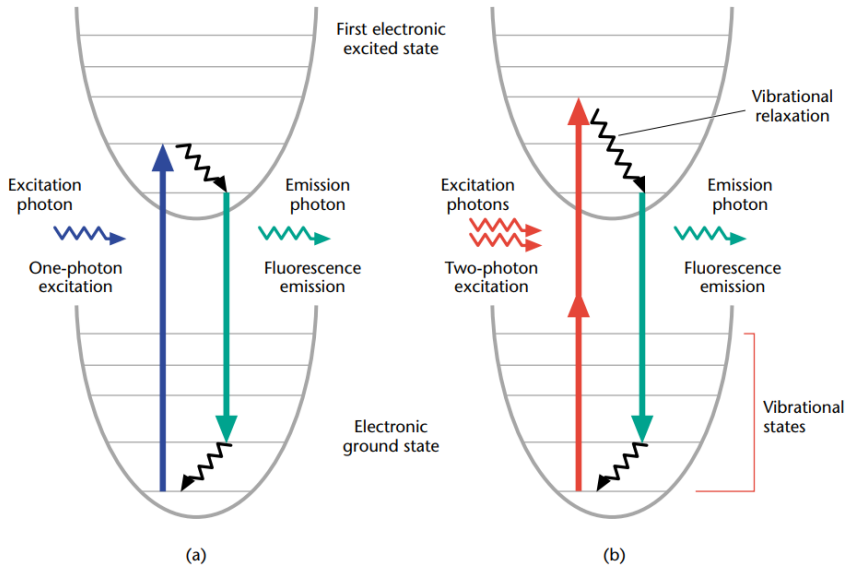

Figure 1. Jablonski diagrams of (a) one-photon and (b) two-photon excitation resulting in fluorescence events. Depicted is the excitation of fluorophores from the ground state to an excited state via vibrational relaxation to the first electronic excited state. Two-photon excitation involves simultaneous absorption of photons of double wavelength and lower

energy. The fluorescence emission is the same for both methods as the vibrational relaxation is the same. Figure taken from So 2002, *Encyclopedia of Life Sciences.*[10]

The goal of this study was to investigate possible cellular metabolic changes that accompany Acid X treatment, in a mouse fibroblast model, utilizing TPEF, the optical redox ratio (**Equation 1**), and fluorescence lifetime imaging (FLIM).

$$\frac{FAD}{(NADH + FAD)} \qquad \textbf{(Eq. 1)}$$

The redox ratio of FAD/(NADH+FAD) is a normalized optical biomarker of relative fluorescence intensities that quantifies metabolism via the autofluorescent cofactors, NADH and FAD, which are omniprevalent in glycolysis, the TCA cycle, and the electron transport chain (ETC) (oxidative phosphorylation). The use of this ratio to study metabolism has been well demonstrated in vitro[8,11–15] and in vivo,[16,17] and its application is useful to discriminate whether the state of a cell is primarily undergoing glycolysis or oxidative phosphorylation. This distinction provides an understanding of the energetic dynamics occurring within a cell exposed to certain conditions, and using TPEF, this can be achieved without the need for a fluorescent tag. As endogenous fluorophores (biological structures that naturally emit light when excited), both NADH and FAD serve as autofluorescent biomarkers of metabolism in the cell. For all practical purposes, the quantum yields (and therefore fluorescence intensities) of NADH and FAD are considered to be dominant to those of their oxidized (NAD^+) and reduced ($FADH_2$) forms, which are quenched and do not exhibit fluorescence.[8] Therefore, normally only NADH and FAD are considered when monitoring autofluorescence and constitute the components of the redox ratio.

Time-correlated single photon counting (TCSPC) fluorescence lifetime imaging (FLIM) is an optical imaging technique that creates an image from the lifetime of the fluorophore signal, rather than the signal intensity. Fluorescence lifetime is defined as the amount of time a fluorophore spends in the excited state before falling back down to ground state, and this can be technically realized using a pulsed light source and single-photon detectors such as photomultiplier tubes (PMTs). In TCSPC, "start" and "stop" signals are defined by the electronics controlling the laser and the single-photon detectors, and a time delay is measured repeatedly at picosecond temporal resolution. These measurements are constructed into a histogram of emission occurrence with respect to time after the excitation pulse.[18] Photon arrival times at the detector are attributed to each pixel and this generates a FLIM image.[18]

FLIM is useful for studying biological samples because of its sensitivity to measuring fluorophores in the environment, independent of detector gain and laser intensity.[19] Because the acquisition time is longer compared to other techniques, FLIM allows for the detection of every photon emitted, and this is useful as fluorescence lifetime is a characteristic unique to each fluorophore. For NADH, FLIM has been used to distinguish between free NADH and protein-bound NADH components as a measure of metabolism.[20–22] These NADH components are recognized as having short and long fluorescence lifetimes, respectively, with variation in long (protein-bound) NADH lifetime that is dependent on the enzyme that NADH binds to, often within the mitochrondria.[23] Therefore, NADH FLIM can serve as a powerful tool to probe the predominant state of NADH in the cell that is tightly correlated to its accepting of electrons in glycolysis or donation of electrons in the ETC. **Equation 2** shows the

biexponential model used to discriminate between short (free) and long (protein-bound) NADH using FLIM. *I(t)* is fluorescence intensity as a function of time, I_0 is initial fluorescence intensity, A_1 is the short (free) NADH relative contribution to total fluorescence, τ_1 is the short (free) NADH lifetime component, A_2 is the long (protein-bound) NADH relative contribution to total fluorescence, and τ_2 is the long (protein-bound) NADH lifetime component.

$$I(t) = I_0(A_1 e^{(-t/\tau_1)} + A_2 e^{(-t/\tau_2)}) \quad \textbf{(Eq. 2)}$$

Considering **Equation 2**, the relative contributions of short and long NADH components to total fluorescence intensity can be described by the ratio of A_1/A_2. In the cellular context, this ratio would be expected to remain constant even as average fluorescence lifetime increases, since only free and protein-bound forms of NADH can ever exist in the cell. This makes A_1/A_2 a microenvironment-independent measure of metabolism using NADH FLIM. This is in contrast to mean fluorescence lifetime that will increase in a microenvironment-dependent manner, meaning that mean lifetime measurements will be sensitive to changes other than metabolism in the cell, such as pH, temperature, and viscosity.[24] These factors should be strongly considered when investigating the administration of an acid to a biological specimen, such as was the case for this study. However, the biexponential equation provides a solution for determining pH-independent metabolic changes through A_1/A_2 for the reasons stated previously. Additionally, the lifetime components, τ_1 and τ_2, provide insight on the resolvable free (short) and protein-bound (long) NADH lifetimes that are thought to be linked to conformational changes associated with binding and unbinding of NADH to different

intracellular enzymes.[8,25] Overall, NADH FLIM is a promisingly powerful method of classifying cellular metabolism that lends specificity to intensity-based measurements such as the redox ratio.

For this study, the optical redox ratio was employed to evaluate possible metabolic changes in live fibroblast cells following administration of increasing Acid X concentration. Additionally, mean lifetime in picoseconds, the A_1/A_2 ratio, and τ_1 and τ_2 in picoseconds were calculated from FLIM images to assess the participation of bound and free NADH. As mentioned previously, since the treatment being evaluated was an acid, it was understood that upon increasing the concentration of acid, the pH of the cellular microenvironment would decrease. Therefore, it was critical to assume that pH could be a confounding variable between Acid X treatment and the observed changes in cellular metabolism. Using acetic acid at increasing concentrations to match the pH values of the Acid X treatments, a pH-control study was carried out that accompanied the Acid X results. Acetic acid was chosen because of its reported role in promoting wound healing.[26] The range of concentrations for Acid X treatment were chosen to capture the percent Acid X (10% w/w) in the sunburn skin care ointment of interest.

2. Methods

2.1. Fibroblast Cell Culture

NIH/Swiss 3T3 fibroblasts, isolated from mouse embryos, were obtained from the ATCC (CRL-1658™; Manassas, VA). The ATCC protocol was referenced for preparation of complete growth medium (DMEM/F-12, Gibco™ supplemented with 10% FBS, no antibiotics), storage, handling of frozen cells, subculturing, and cryopreservation.[27] For imaging and live/dead studies, cells of similar passage number (P 6-8) were used and seeded into sterile and coated 35 mm glass-bottom dishes (P35GC1.514C, MatTek Corporation) at a cell density of approximately 80,000 cells per dish.

2.2. Acid X and Acetic Acid Treatments

For the Acid X treatment, liquid volumes of Acid X were supplemented into fibroblast growth medium at 0, 5, 10, and 15% w/w concentrations. For the pH-control treatment, liquid volumes of ≥99% acetic acid (CAS 64-19-7, Sigma-Aldrich) were supplemented into fibroblast growth medium to match the pH values of Acid X in media at 0, 5, 10, and 15% w/w concentrations, which were 7.65, 2.39, 2.03, and 1.85, respectively. The untreated control groups of 0% w/w Acid X (pH 7.65) and 0% w/w acetic acid (pH 7.65) consisted of media only. The pH of each treatment concentration was acquired using a pH meter (Orion Star™ A211, Thermo Scientific™). Treatments were directly pipetted into 35 mm glass-bottom dishes, containing adhered fibroblasts, and were imaged at 0 hour post-treatment. This imaging timepoint was chosen based on a

preliminary study with pig skin conducted by Hallie Ramser Toomer. All samples were prepared in triplicate for both studies.

2.3. Live/Dead Cell Assay

NucGreen® Dead 488 ReadyProbes® Reagent (R37109, Invitrogen™) was used to assess the ratio of live/dead cells upon Acid X and acetic acid treatments of pH 2.03 compared to the control (pH 7.65). At 0 hour post-treatment, the stain was added to each sample dropwise at a concentration of 2 drops/mL of media and was allowed to incubate for 10 minutes prior to imaging. Images were acquired using an Olympus Fluoview FV10i-LIV inverted laser scanning confocal microscope (Olympus Life Science, Waltham, MA) and a 60x water-immersion objective (Olympus, 1.2 NA). Live cell imaging was facilitated by use of a built-in microincubator to maintain temperature (37 °C), humidity (>90%), and CO_2 (5%). Live and dead cells were counted manually at 3 regions of interest (ROI) for each dish to obtain a live/dead ratio. No dish replicates were prepared as this was a pilot study.

2.4. In Vitro Two-Photon Excited Fluorescence Imaging

For live cell TPEF imaging, a Bruker Ultima Investigator Series multiphoton microscope (Spectra Physics, Santa Clara, CA) equipped with a microincubation chamber for temperature (37 °C) and humidity control, accompanied by a rigid stand and platform (MP200, Thorlabs, Inc.) for inverted configuration imaging was used. A Ti:Sapphire laser (Mai Tai, Spectra Physics) provided a continuous power source (690-1040 nm) and

a Pockels cell (Thorlabs, Inc.) was used for beam control. A 20x water-immersion objective (Olympus, 1.2 NA) was used with ultrasound gel to acquire all images at a 2.0x digital magnification. The laser scanning mode in the Prairie View Software was set to Galvo. A schematic of the optical instruments used is shown below (**Figure 2**). Dichroic beamsplitters (Chroma, T495lpxr) filtered out wavelengths of light before they reached 460(±20) nm (Chroma, ET460/40m-2p) and 525(±20) nm (Chroma, ET460/50m-2p) GaAsP photomultiplier tube (PMT) emission filters that were used to detect NADH and FAD fluorescence, respectively. The PMT gains were determined upon imaging the first control replicate and were kept the same throughout each study. Incident power on the cells, measured at the objective lens, never exceeded 50 mW. For each sample, images (512 x 512 pixels for Acid X study, 1024 x 1024 for pH study; 12-bit depth) were acquired at 3 ROIs at excitation wavelengths of 755 nm for NADH fluorescence and 855 nm for FAD fluorescence.

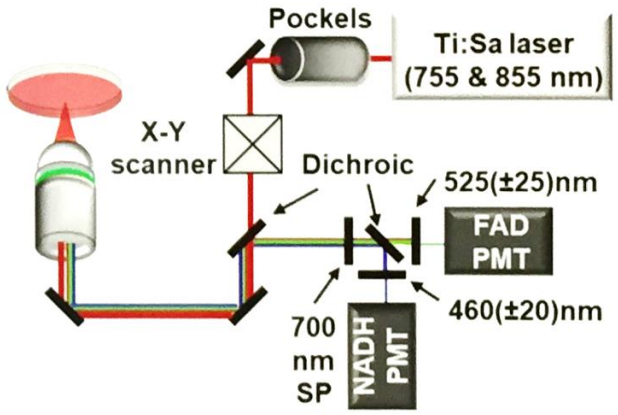

Figure 2. Schematic of inverted multiphoton microscope and optical instruments setup for in vitro live-cell imaging in the Quinn Lab. Photo courtesy of Olivia Kolenc.

2.5. In Vitro Fluorescence Lifetime Imaging

Using the FLIM acquisition mode on the MPM, images at 755 nm were taken to distinguish free and bound components of NADH. 512 x 512 NADH lifetime images were generated by detecting photons per pixel emitted over 2 minutes of a pulsing excitation source. The number of photons that hit the detector are directly related to the objective power used to excite the sample. Time delay measurements between "start" and "stop" times of excitation-emission events were constructed as a histogram to which the biexponential decay function (**Equation 2**) was fit using SPCImage software (ver 7.4; Becker & Hickl GmbH; Berlin, Germany). A pixel dwell time of 4.8 μs was used as well as an objective power that never exceeded 50 mW. 3 ROIs were acquired per dish.

2.6. Data Interpretation

2.6.1. Calculation of Optical Redox Ratio

Laser power readings were acquired each day of imaging to normalize fluorescence intensities and account for instrumental variability. The Matlab code to perform batch image analysis for the optical redox ratio of FAD/(NADH+FAD) was written by Hallie Ramser Toomer and Jake Jones. Redox ratio maps were calculated using pixels from the entire image and the jet color map in Matlab was applied to show a color gradient from 0 to 1. Standard deviations of the redox ratio within triplicates and between groups were calculated to assess reliability and precision of each sample measurement. Box-and-whisker plots for the distribution of data were created in Microsoft Excel.

2.6.2. FLIM Analysis

All FLIM images were processed using SPCImage software (ver 7.4; Becker & Hickl GmbH; Berlin, Germany). The instrument response function (IRF) was set for each image by loading the second harmonic signal from urea crystals. A pixel of representative photon counts was manually picked for further analysis. Binning was set to 2 to obtain pixel photon counts of approximately 10,000 for each image and an incomplete multi-exponential model was used. Appropriate fit to the histogram plots were determined by chi-squared values of <1.5. Mean lifetime (ps), A_1/A_2, and τ_1 and τ_2 calculations were acquired using a FLIM code for Matlab written by Hallie Ramser Toomer. Mean lifetime (ps) and A_1/A_2 maps were also constructed using this Matlab code. Box-and-whisker plots for the distribution of data were created in Microsoft Excel.

2.6.3. Statistical Analysis

Differences in redox ratio, mean lifetime (ps), A_1/A_2 ratio, and τ_1 and τ_2 were tested for statistical significance using Tukey's HSD post hoc test, where $p < 0.05$ for comparisons between pairs was considered statistically significant. Tukey's HSD test was chosen instead of Student's t test to control for the error rate per-experiment. One way analysis of variance (ANOVA) analysis was run to assess variation between treatment groups within each study. All analysis was carried out in JMP Pro 14 (SAS Institute Inc.; Carry, NC).

3. Results and Discussion

3.1. Optical redox ratio may quantify Acid X-induced cellular metabolic changes in vitro in a concentration-dependent manner.

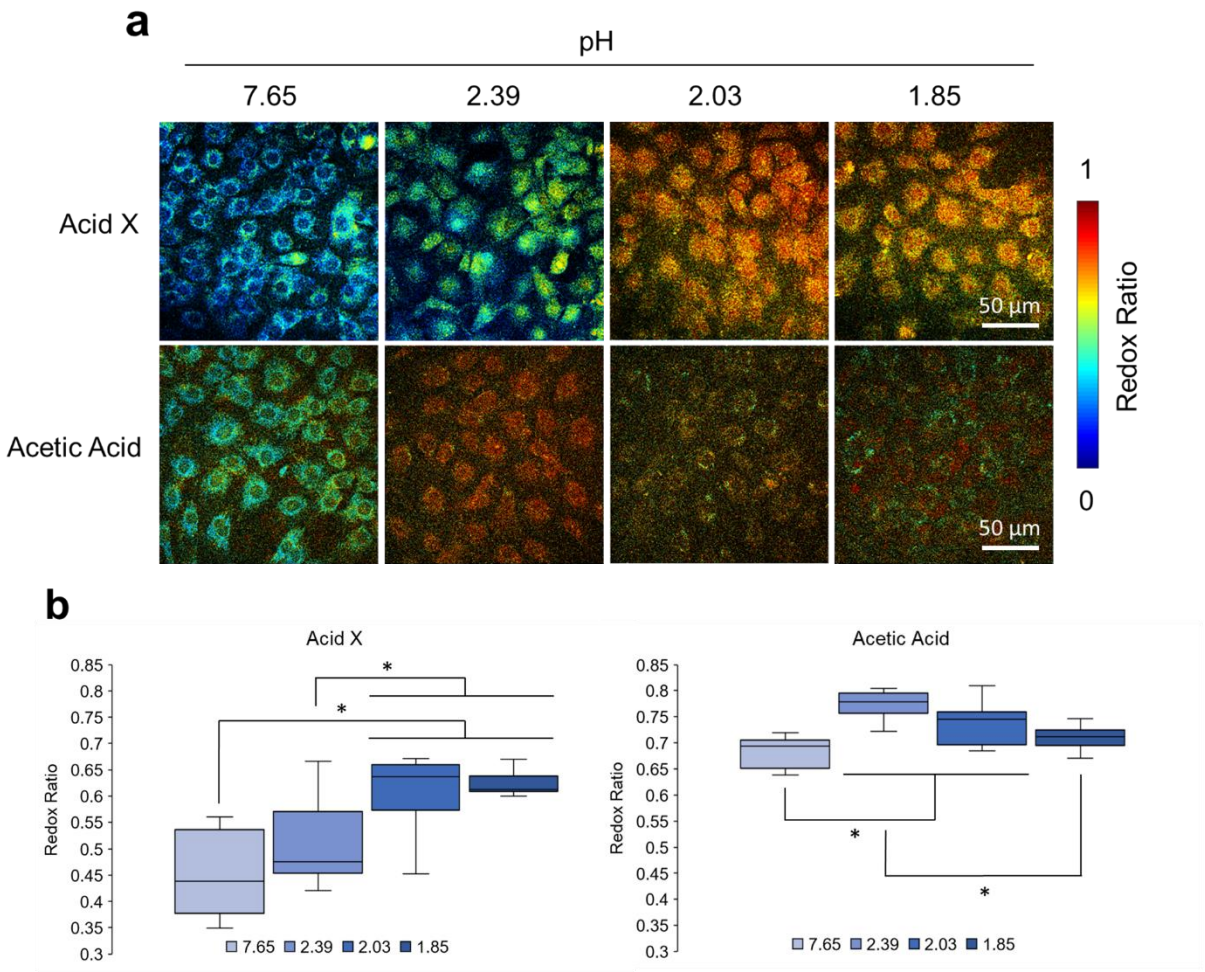

Figure 3. Optical redox ratio for increasing Acid X and Acetic Acid concentrations. **a** Representative redox ratio maps were generated from normalized fluorescence intensities of FAD/(NADH+FAD) at each pixel. **b** Redox ratio was calculated per image by averaging per pixel fluorescence intensity over the entire image. The redox ratios of the pH 2.03 and 1.85 Acid X groups were significantly increased compared to the controls ($p = 0.0002$) and to the pH 2.39 Acid X group ($p = 0.0216$, $p = 0.0174$). The redox ratios of the pH 2.39 and 2.03 Acetic Acid groups were significantly increased compared to the controls ($p < 0.001$, $p = 0.0005$) and the redox ratio of the pH 1.85 group was significantly decreased compared to that of the pH 2.39 group ($p = 0.0017$). The line inside each box represents the median, the bounds of the boxes are the 25th and 75th quantiles, and the whiskers extend to the full range of the data.

Using the optical redox ratio of FAD/(NADH+FAD) to assess changes in cellular metabolism, it was observed that the ratio increased for the 10 and 15% w/w Acid X (pH 2.03 and 1.85) groups compared to the controls ($p = 0.0002$) and compared to the 5% w/w Acid X (pH 2.39) group ($p = 0.0216$, $p = 0.0174$). A higher redox ratio suggests that more NAD^+ is present in the cells relative to NADH, indicating increased oxidative phosphorylation relative to glycolysis (**Figure 3b**). A different trend in redox was observed for the acetic acid study. The redox ratio increased significantly between the pH of 2.39, 2.03, and control groups ($p < 0.001$, $p = 0.0005$) representing the 5, 10, and 0% w/w Acid X groups, respectively, and decreased for the pH of 1.85 group ($p = 0.0017$) compared to the pH of 2.39 group (**Figure 3b**). A decrease in redox ratio is expected to indicate more relative NADH present in the cells as glycolytic activity is increased relative to ETC activity.

Observing an increase in redox ratio for the Acid X study is revealing because it is known that Acid X topical treatment can result in chemical peeling, keratinocyte proliferation, and collagen thickening. The different trends for these two studies warrant consideration of the possibility that multiple biological factors, in addition to Acid X concentration and pH, may affect the optical redox ratio. A two-way (factorial) ANOVA was carried out to test the interaction between acid type and pH on the redox ratio (Error! Reference source not found.).

Table 1. Two-way ANOVA effects test results using JMP Pro 14.

	DF	Sum of Squares	F Ratio	Prob > F
Acid Type	1	0.5876	203.6	<0.0001
pH	3	0.1572	18.16	<0.0001
Acid Type*pH	3	0.0929	10.72	<0.0001

Results showed that the average redox ratios for acid type and pH were significantly different from one another, and that the value of the redox ratio was influenced by an interaction between acid type and pH (**Error! Reference source not found.**). This statistical analysis supports the observation that the overall distribution of redox ratio values was higher for acetic acid concentrations compared to Acid X concentrations. However, the redox ratio value for the untreated controls in both studies should be the same, although this was not observed. This discrepancy may be explained by the possibility of carbon channeling to other biosynthetic pathways, such as the pentose phosphate pathway or fatty acid synthesis, which cannot be accounted for by the redox ratio.[8]

The increasing optical redox ratio for the Acid X treatment condition hints at an increased demand for an efficient means of energy production via the ETC. If the accompanying acetic acid study had shown a similar trend in redox, it might be possible that pH changes were more influential in changing the redox ratio than the Acid X treatment itself. To investigate pH as a potential confounding variable, FLIM analysis, as an intensity independent measure of NADH lifetime, was conducted.

3.2. NADH FLIM suggests that cellular metabolic changes due to Acid X treatment in vitro occur in a pH-independent manner.

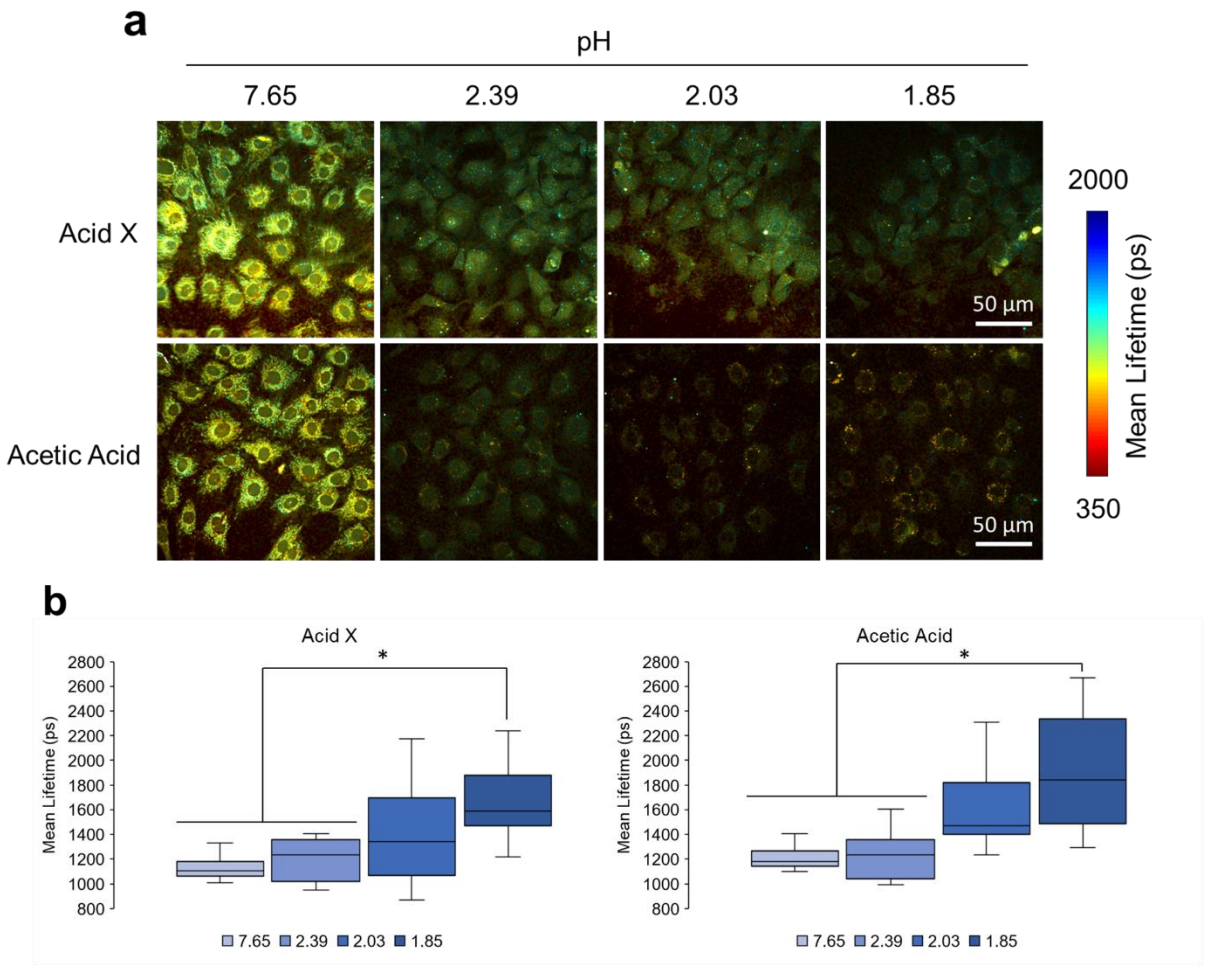

Figure 4. Mean lifetime (ps) for increasing Acid X and Acetic Acid concentrations. **a** Representative mean lifetime maps were generated from fitting the biexponential model, $I(t)=I_0(A_1e^{(-t/\tau 1)}{}_+ A_2e^{(-t/\tau 2)})$, to the histogram at each pixel. **b** Mean lifetime was calculated for each image by averaging initial fluorescence intensity I_0 over the entire image. Mean lifetime of the pH 1.85 Acid X group was significantly increased compared to the controls ($p = 0.0039$) and to the pH 2.39 Acid X group ($p = 0.0108$). A similar trend was seen in the Acetic Acid concentration study as the mean lifetime of the pH 1.85 group was significantly increased compared to the controls ($p = 0.0014$) and to the pH 2.39 group ($p = 0.0007$). The line inside each box represents the median, the bounds of the boxes are the 25^{th} and 75^{th} quantiles, and the whiskers extend to the full range of the data.

Using **Equation 2** to calculate the mean lifetime for each image, it was found that the 15% w/w Acid X (pH 1.85) group mean lifetime was increased compared to the controls ($p = 0.0039$) and to the 5% w/w Acid X (pH 2.39) group ($p = 0.0108$). For the corresponding acetic acid study, a similar trend for mean lifetime showed that the pH 1.85 group had an increased mean lifetime compared to the controls ($p = 0.0014$) and to the pH 2.39 group ($p = 0.0007$) (**Figure 4b**). The increase in mean lifetime corresponding to increasing Acid X concentration (and therefore decreasing pH) was as expected since longer mean lifetime has been associated with a high redox ratio and a shorter mean lifetime with a low redox ratio.[8,16] However, the opposite relationship between redox and mean lifetime has also been reported in cancer treatment studies.[8]

The complexity of interpretation for mean lifetime analysis stems from its sensitivity to factors in the cellular microenvironment (e.g. pH, temperature, and viscosity).[18] Without supporting evidence from negative control variables that control for the disruption of glycolysis or the ETC, a direct relationship between Acid X treatment and metabolic changes is difficult to establish. Research that discriminates mitochondrial respiration regulated by uncoupling proteins and proton efflux (biochemical aspects of ETC activity) may provide additional information regarding the relationship between Acid X dosing and cellular metabolism. In theory, the ratio of A_1/A_2 is expected to be sensitive to only changes in metabolism and can overcome this issue.[8]

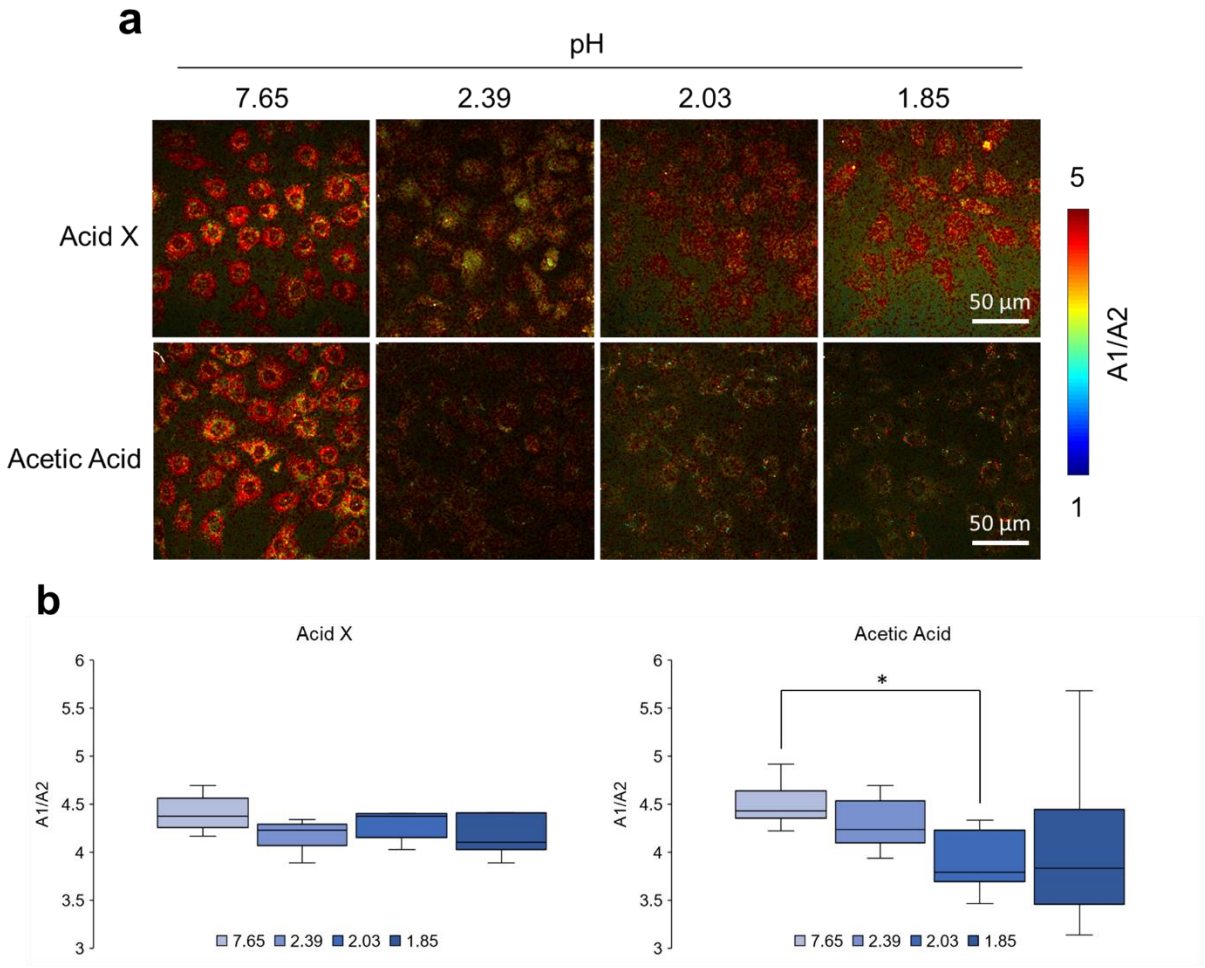

Figure 5. NADH lifetime ratio (A_1/A_2) for increasing Acid X and Acetic Acid concentrations. **a** Representative A_1/A_2 maps reveal pH-independent changes in the relative fluorescence contributions of free (A_1) and protein-bound (A_2) NADH components to total fluorescence. **b** A_1/A_2 calculated for each image show that the contributions to NADH lifetime remained significantly consistent for all Acid X treatment concentrations, while there was a significant decrease in A_1/A_2 between the Acetic Acid pH 2.03 group and controls ($p = 0.0173$). The line inside each box represents the median, the bounds of the boxes are the 25th and 75th quantiles, and the whiskers extend to the full range of the data.

Analysis of the free and bound NADH lifetime components shows that the ratio of A_1/A_2 remains consistent across all concentrations for the Acid X study (**Figure 5b**). This data indicates that the relative fluorescence contributions from both free and protein-

bound NADH lifetime components is similar in cells both with and without the administration of Acid X. However, it was expected that A_1/A_2 would show a decrease to match the increase observed in the redox ratio for the Acid X study. This would be indicative of increased complex I-bound NADH in the ETC, located within the mitochondria. A decrease in A_1/A_2 ratio between the control and acetic acid pH 2.03 group was observed and matches this hypothesis. A high A_1/A_2 ratio, on the other hand, which was not observed, has been associated with a low redox ratio and its associated changes in cellular respiration.[8]

It is interesting that no change was seen in A_1/A_2 for increasing concentrations of Acid X, although significant increases in the optical redox ratio were observed (**Figure 3**). This unexpected invariance may be explained by the limitation of the biexponential model (**Equation 2**) that does not account for NADH binding to a variety of enzymes in the cell.[8] It has been previously reported in mouse cerebral tissue that 4 distinct NADH lifetime components were observed when bottlenecks were introduced in specific metabolic pathways, compared to baseline metabolic activity.[25] This research suggests that when NADH binds to binding sites on specific enzymes, the action may result in conformational changes that are resolved as distinct fluorescence lifetimes. Based on this hypothesis, it may be assumed that a change in A_1/A_2 was not observed for increasing Acid X concentrations due to unresolved NADH binding to different enzymes, that when aggregated, did not change the free-to-bound ratio. However, more work needs to be done to separate out the emission wavelengths that distinguish the types of enzymes that NADH may bind to.

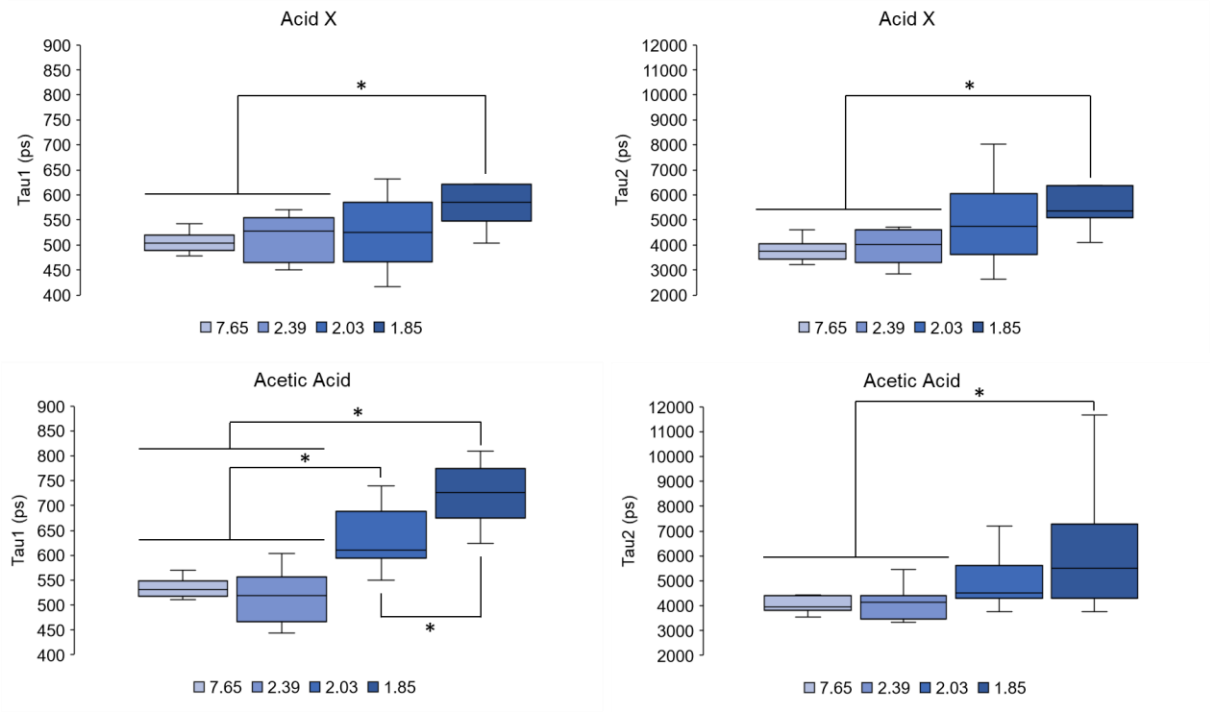

Figure 6. Tau_1 (τ_1) and Tau_2 (τ_2) values for increasing Acid X and Acetic Acid concentrations. For increasing Acid X concentration, τ_1 increased significantly between the 15% w/w Acid X (pH 1.85) group and the control and 5% w/w Acid X (pH 2.39) groups ($p = 0.0351$, $p = 0.0489$). For increasing Acetic Acid concentration, τ_1 increased significantly between the pH 1.85 and 2.03 groups and the control and pH 2.39 groups ($p \leq 0.0002$), as well as between the pH 1.85 and pH 2.03 groups ($p = 0.0158$). τ_2 increased significantly between the control and pH 2.39 groups and the pH 1.85 group for both Acid X and Acetic Acid concentrations. ($p = 0.0273$, $p = 0.0258$, $p = 0.0175$, $p = 0.0248$). The line inside each box represents the median, the bounds of the boxes are the 25^{th} and 75^{th} quantiles, and the whiskers extend to the full range of the data.

Similar to mean lifetime, the values of τ_1 and τ_2 are expected to be influenced by environmental pH changes, according to **Equation 2**. Based on the graphs in **Figure 6**, for both Acid X and acetic acid treatments, τ_1 and τ_2 increased significantly compared to the control. Across all treatment concentrations, the greatest increase in τ_1 and τ_2 lifetimes was observed for an environmental pH of 1.85 compared to the no treatment control. These add specificity to the mean fluorescence lifetime data presented in **Figure 4** and

discussed previously. Particularly, it was observed that the range of lifetimes for the τ_1 (short) NADH component for acetic acid was higher than that observed for Acid X. This agrees with the higher range of mean lifetime observed for the acetic acid treatments (**Figure 4**). This could potentially mean that the environment surrounding the acetic acid-treated cells was more acidic than the measurements indicate. However, acetic acid is a weaker acid with a higher pK_a value compared to Acid X. It is therefore more reasonable to assume that the variability in pH might have been greater between samples treated with acetic acid, in comparison to those treated with the stronger acidifier, Acid X. The similar values for τ_2 between the Acid X and acetic acid studies may be explained by the ability of NADH to bind to different intracellular enzymes and take on multiple conformations.

3.3. Cell viability is not compromised by chosen Acid X and Acetic Acid concentrations.

Changes in autofluorescence between control and Acid X-treated groups were measured by an increase in the redox ratio, which was corroborated by an increase in mean lifetime using FLIM. In contrast, clear consistency of interpretation between redox and FLIM data was not observed for the acetic acid study. To validate the observed redox ratio and FLIM results, it was critical to validate the living state of the fibroblast cells under the Acid X and acetic acid treatment concentrations.

Although acetic acid has been reported to play a role in the healing of wounds caused by bacteria,[26] mixed findings have been reported concerning the effects of acetic acid on fibroblast cultures.[28,29] Nagoba et al. advocates for the use of acetic acid as a treatment for bacterial infection without any toxic side effects, and claims that in vitro

studies indicating acetic acid toxicity in fibroblasts are not decisive.[28]Additionally, Okabe et al. shows that acetic acid can be used to cause cell death of cancer cells, therefore acting as an anticancer agent.[29] A pilot live/dead cell viability assay was carried out for 10% w/w Acid X (pH 2.03), corresponding acetic acid treatment (pH of 2.03), and untreated control to validate the use of acetic acid in this study. The results showed no significant differences in the ratios of live/dead cells across all groups (**Figure 7**).

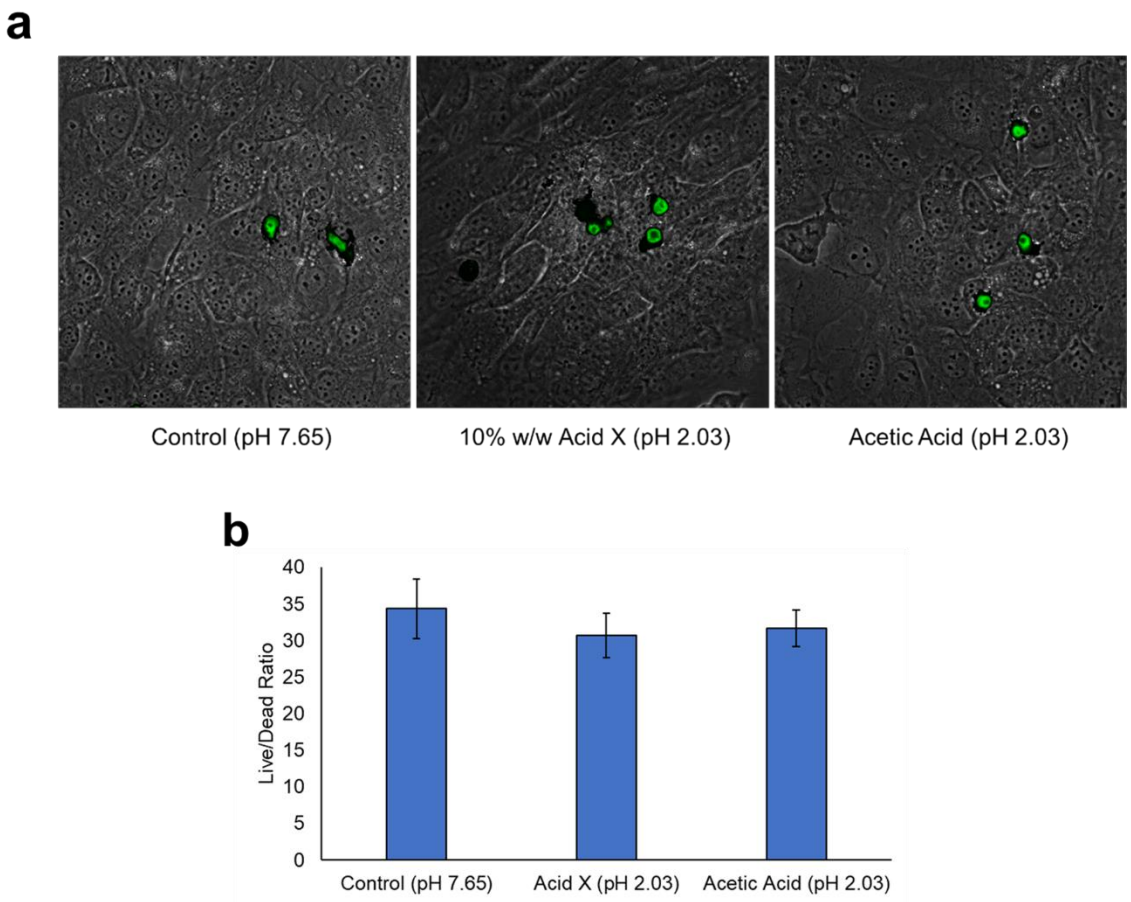

Figure 7. Live/Dead cell viability for validation of Acid X and Acetic Acid concentrations at pH 2.03. **a** Representative confocal microscopy images of cells stained with NucGreen™ Dead 488 ReadyProbes® reagent (R37109, Invitrogen™). Green fluorescence indicates dead cells that have damaged plasma membranes and DNA leakage. **b** Live/Dead ratio was calculated by averaging cell counts over 3 ROIs per dish. Standard error bars indicate no significant differences between groups.

Additional methods of analysis are required to fully understand the effects of acetic acid on the physiology of fibroblasts and how this relates to metabolic changes. The sharp increase followed by a decrease in redox observed for increasing acetic acid concentration (**Figure 3b**) indicated that the catabolism of carbon substrates via the ETC might be reduced relative to glycolytic activity. However, acetic acid has been classified as an inhibitor of carbohydrate metabolism,[30] for which the redox ratio would be expected to increase, showing preference for NAD^+ over NADH. One explanation for this discrepancy is that the imaging timepoint of 0 hours post-treatment was too short of an incubation time to catch the full effect of acetic acid on metabolism, which may occur over an extended period of time in the cell.

4. Conclusions

In these studies, I was able to investigate autofluorescence of the metabolic cofactors, NADH and FAD, in vitro, under Acid X and acetic acid treatments by utilizing TPEF, the optical redox ratio, and FLIM. The optical redox ratio is a well understood method of quantitatively assessing cellular metabolism in vitro, and these results show support for an Acid X concentration-dependent increase in redox ratio. These results imply that metabolism involving increased levels of NADH, relive to NAD^+, occur in fibroblasts post-Acid X administration, and this may be the result of increased ETC activity relative to glycolysis. FLIM mean lifetime analysis presented itself similarly across both Acid X and acetic acid treatments, in agreement with the high redox ratio results. The A_1/A_2 ratio decreased significantly in agreement with the observed redox ratio for increasing acetic acid treatment only. The lack of a similar trend in A_1/A_2 for

increasing Acid X concentration may be explained by the limitations of the biexponential decay to distinguish between different enzyme binding and subsequent conformations of NADH. The values of τ_1 and τ_2 confirmed the influence of pH observed in the mean lifetime analysis, although it is unsure how these results come together to explain changes in cellular metabolism. Finally, the cell viability study validated the concentrations of Acid X and acetic acid used in these experiments to evaluate metabolism in living cells. Together, the application of methods here demonstrates that autofluorescence optical imaging by TPEF can be used to evaluate Acid X treatment response in live cells, in a dose dependent manner.

5. Future Work

In vitro work was a first step in evaluating the effects of the topical application of Acid X to skin as a treatment for sunburns. Experiments that utilize an in vitro 3D human skin model (EpiDerm^{TM}, MatTek) to study UV-induced sunburns and application of topical skin ointment, containing Acid X, have been carried out, and data processing is ongoing. A future goal is to replicate the preliminary results in a mouse model (Animal Use Protocol has been submitted and accepted) for further validation of Acid X treatment administration in humans. Additionally, use of these advanced experimental model systems will allow for depth section imaging that has the power to evaluate drug delivery mechanisms using quantitative optical imaging. All future work will allow closer evaluation of how sunburn skin ointments may interact metabolically with sunburns in human tissue.

REFERENCES

1. The American Cancer Society, Inc. UV Radiation | The Cancer Atlas. in (2014).
2. Ulff, E., Maroti, M., Serup, J., Nilsson, M. & Falkmer, U. Prophylactic treatment with a potent corticosteroid cream ameliorates radiodermatitis, independent of radiation schedule. *Radiother. Oncol.* **122**, 50–53 (2017).
3. Li, H. *et al.* Protective Effect of Curcumin Against Acute Ultraviolet B Irradiation-induced Photo-damage. *Photochem. Photobiol.* **92**, 808–815 (2016).
4. Wu, G. X., Huang, H. H., Chang, H. R. & Kuo, S. M. Evaluation of the UVB-screening capacity and restorative effects exerted by farnesol gel on UVB-caused sunburn. *Environ. Toxicol.* **33**, 488–507 (2018).
5. Reich, H., Wallander, I. & Schulte, L. Comparative Study of Professional vs Mass Market Topical Products for Treatment of Facial Photodamage. *J. Drugs Dermatol.* **15**, (2016).
6. Spectra-Physics. Mai Tai Data Sheet: Ultrafast One Box TI:Sapphire Lasers. (2018).
7. Georgakoudi, I. & Quinn, K. P. Optical Imaging Using Endogenous Contrast to Assess Metabolic State. *Annu. Rev. Biomed. Eng.* **14**, 351–367 (2012).
8. Kolenc, O. I. & Quinn, K. P. Evaluating Cell Metabolism Through Autofluorescence Imaging of NAD(P)H and FAD. *Antioxid. Redox Signal.* **30**, 875–889 (2019).
9. Rubart, M. Two-Photon Microscopy of Cells and Tissue. *Circ. Res.* **95**, 1154–1166 (2004).
10. So, P. T. Two-photon Fluorescence Light Microscopy. *Encycl. Life Sci.* (2002).

11. Alhallak, K., Rebello, L. G., Muldoon, T. J., Quinn, K. P. & Rajaram, N. Optical redox ratio identifies metastatic potential-dependent changes in breast cancer cell metabolism. *Biomed. Opt. Express* **7**, 4364 (2016).

12. Wallrabe, H. *et al.* Segmented cell analyses to measure redox states of autofluorescent NAD(P)H, FAD & Trp in cancer cells by FLIM. *Sci. Rep.* **8**, (2018).

13. Blacker, T. S. & Duchen, M. R. Investigating mitochondrial redox state using NADH and NADPH autofluorescence. *Free Radic. Biol. Med.* **100**, 53–65 (2016).

14. Ostrander, J. H. *et al.* Optical Redox Ratio Differentiates Breast Cancer Cell Lines Based on Estrogen Receptor Status. *Cancer Res.* **70**, 4759–4766 (2010).

15. Chen, L.-C. *et al.* Nonlinear optical molecular imaging enables metabolic redox sensing in tissue-engineered constructs. in (eds. Lin, C. P. & Ntziachristos, V.) 80890J (2011). doi:10.1117/12.889713

16. Jones, J. D., Ramser, H. E., Woessner, A. E. & Quinn, K. P. In vivo multiphoton microscopy detects longitudinal metabolic changes associated with delayed skin wound healing. *Commun. Biol.* **1**, (2018).

17. Quinn, K. P. *et al.* Diabetic Wounds Exhibit Distinct Microstructural and Metabolic Heterogeneity through Label-Free Multiphoton Microscopy. *J. Invest. Dermatol.* **136**, 342–344 (2016).

18. Trautmann, S. *et al.* Fluorescence Lifetime Imaging (FLIM) in Confocal Microscopy Applications: An Overview. 14

19. Becker, W. Introduction to Multi-dimensional TCSPC. in *Advanced Time-Correlated Single Photon Counting Applications* (ed. Becker, W.) **111**, 1–63 (Springer International Publishing, 2015).

20. Lakowicz, J. R. Fluorescence lifetime imaging of free and.protein-bound NADH Proc. Nati. Acad. Sci. USA Vol. 89, pp. 1271-1275, February 1992 Biochemistry. 5

21. Guo, H.-W. *et al.* Correlation of NADH fluorescence lifetime and oxidative phosphorylation metabolism in the osteogenic differentiation of human mesenchymal stem cell. *J. Biomed. Opt.* **20**, 017004 (2015).

22. Meleshina, A. V. *et al.* Two-photon FLIM of NAD(P)H and FAD in mesenchymal stem cells undergoing either osteogenic or chondrogenic differentiation. *Stem Cell Res. Ther.* **8**, (2017).

23. Skala, M. C. *et al.* In vivo multiphoton fluorescence lifetime imaging of protein-bound and free nicotinamide adenine dinucleotide in normal and precancerous epithelia. *J. Biomed. Opt.* **12**, 024014 (2007).

24. Chen, L.-C. *et al.* The potential of label-free nonlinear optical molecular microscopy to non-invasively characterize the viability of engineered human tissue constructs. *Biomaterials* **35**, 6667–6676 (2014).

25. Yaseen, M. A. *et al.* Fluorescence lifetime microscopy of NADH distinguishes alterations in cerebral metabolism in vivo. *Biomed. Opt. Express* **8**, 2368 (2017).

26. Basavraj S., N., Namdev M., S., Bharat, W. & Sahon, S. Acidic Environment and Wound Healing: A Review. *WOUNDS* **27**, 5–11 (2015).

27. American Type Culture Collection (ATCC). ATCC Product Sheet NIH/3T3 (ATCC CRL-1658).

28. Nagoba, B. S., Selkar, S. P., Wadher, B. J. & Gandhi, R. C. Acetic acid treatment of pseudomonal wound infections – A review. *J. Infect. Public Health* **6**, 410–415 (2013).

29. Okabe, S., Okamoto, T., Zhao, C.-M., Chen, D. & Matsui, H. Acetic acid induces cell death: An *in vitro* study using normal rat gastric mucosal cell line and rat and human gastric cancer and mesothelioma cell lines: Acetic acid induces cell death. *J. Gastroenterol. Hepatol.* **29**, 65–69 (2014).

30. Acetic Acid (Code C61623). *NCI Thesaurus* Available at: URL:https://ncit.nci.nih.gov/ncitbrowser/ConceptReport.jsp?dictionary=NCI_Thesaurus&ns=ncit&code=C61623.